

The Northern Fish Lake Valley Pull-Apart Basin: Geothermal Prospecting with Hyperspectral Imaging

B.A. Martini, P. Hausknecht, W.L. Pickles

This article was presented at Geothermal Resources Council 2004 Annual Meeting, Palm Springs, CA, Aug 29 – Sep 1, 2004

March 3, 2004

U.S. Department of Energy

Lawrence
Livermore
National
Laboratory

DISCLAIMER

This document was prepared as an account of work sponsored by an agency of the United States Government. Neither the United States Government nor the University of California nor any of their employees, makes any warranty, express or implied, or assumes any legal liability or responsibility for the accuracy, completeness, or usefulness of any information, apparatus, product, or process disclosed, or represents that its use would not infringe privately owned rights. Reference herein to any specific commercial product, process, or service by trade name, trademark, manufacturer, or otherwise, does not necessarily constitute or imply its endorsement, recommendation, or favoring by the United States Government or the University of California. The views and opinions of authors expressed herein do not necessarily state or reflect those of the United States Government or the University of California, and shall not be used for advertising or product endorsement purposes.

This is a preprint of a paper intended for publication in a journal or proceedings. Since changes may be made before publication, this preprint is made available with the understanding that it will not be cited or reproduced without the permission of the author.

This work was performed in part under the auspices of the U.S. Department of Energy by the University of California, Lawrence Livermore National Laboratory under Contract No. W-7405-Eng-48.

The Northern Fish Lake Valley Pull-Apart Basin: Geothermal Prospecting with Hyperspectral Imaging

B. A. Martini¹, P. Hausknecht¹, W. L. Pickles²,

¹ HyVista Corporation, Sydney, NSW, 2113, Australia

² Lawrence Livermore National Laboratory, Livermore, CA, 95007, USA

ABSTRACT

High fidelity continuous surface mineralogy maps are combined with local and regional structural models in order to define/refine exploration targets in Fish Lake Valley, NV. Surface mineralogy is derived from a 400 km² airborne hyperspectral survey collected in July 2003. Smart and efficient first-tier algorithms consisting primarily of band indices were developed to process and “spectrally strain” the large dataset for zones of prospective mineral assemblages. The reduced mineral targets then endured re-processing with more sophisticated spectral identification and mapping algorithms. A site at the intersection of the east-trending Coaldale Fault and north-northeast-trending Emigrant Peak Fault Zone was delineated and re-processed for further spectral identification. Populations of montmorillinite, kaolinite, jarosite, alunite and pyrophyllite in this region indicate anomalous geothermal gradients now or in the past and sustained hydrothermal discharge along faults, fractures and contacts in far northeastern Fish Lake Valley. Increased permeability and higher geothermal inputs at this locale are likely due to the transtensional deformation that focuses in this portion of the major right-stepover of the central Walker Lane deformation belt.

Keywords

Hyperspectral, Fish Lake Valley, Coaldale Fault, Emigrant Peak Fault Zone, Walker Lane

INTRODUCTION

Though explored in the recent past, Fish Lake Valley remains an unexploited and under-characterized geothermal province in the greater Basin and Range. Fusion of recent regional and tectonic models with high spatial and spectral resolution hyperspectral data provides a new framework for targeting zones of flow and discharge in the Fish Lake Valley region. The change from regional extension in the Miocene to predominately transcurrent faulting in the Pliocene to recent has made timing, type and amount of crustal displacement ambiguous and renders model-driven geothermal exploration in the region more difficult.

Continuous surface mineralogy maps derived from hyperspectral data have proven quite useful in other geothermal locales (Long Valley Caldera, Dixie Valley, Brady-Desert Peak, etc.). These maps, when combined with known geology, help to create system-wide maps of both possible discharge conduits and zones experiencing little to no discharge. Last year’s HyMap survey was flown in hopes of utilizing the above fusion techniques in constraining new exploration targets for the region.

NORTHERN FISH LAKE VALLEY PULL-APART BASIN

Fish Lake Valley is located in far western Nevada and is bounded to the west by the White Mountains and to the east by the Silver Peak Range (see Figure 1B).

Figure 1A.. Location of Fish Lake Valley within the regional-scale tectonic regime (modified from Reheis and Sawyer, 1997). Dashed polygon shows extent of figure 1B. **B.** Close-up of structure bounding the northern Fish Lake Valley pull-apart basin (modified from Stockli et al., 2003). Dashed polygon shows boundary of HyMap hyperspectral survey.

The northwest-trending Fish Lake Valley Fault Zone (FLVFZ) forms its western boundary. Extension initiated on this structure sometime in the middle Miocene (ca. 12 Ma) and was jointly accommodated in the region by the Mineral Ridge detachment located to the east in the Silver Peak Range (Stockli et al., 2003). After rapid extension, continent-scale Eastern California Shear Zone (ECSZ) deformation began to overprint the Basin and Range normal faults with dextral shear. This change in deformation style reached Fish Lake Valley latitudes at approximately 6 Ma. Andesitic and rhyolitic volcanism initiated in northern Fish Lake Valley in response to this structural change as did formation of the high-angle Emigrant Peak Fault Zone (EPFZ) (Stockli et al., 2003). This normal oblique shear fault transfers slip from the northern FLVFZ northeastwards into the southern-central Walker Lane Belt (WLB), and forms the eastern boundary of the Fish Lake Valley (Figure 1B). The northern boundary is formed by the east-trending Coaldale Fault (CF), which has shifted from a right-lateral accommodation structure in the middle Miocene to a left-lateral transcurrent fault in the present (Stockli et al., 2003) (Figure 1B). It is the major southern structure of the Mina Deflection which transfers shear-oblique slip from the southern faults of the WLB to the northern (Bradley et al., 2003). Normal extension coupled with both right-lateral shear overprinting (on the FLVFZ) and left-lateral shear (on the CF) has conspired to create a classic transtensional pull-apart basin in northern Fish Lake Valley (Figure 1B). This complexity ultimately sets Fish Lake apart from many of its neighboring Basin and Range-hosted geothermal locales.

HYMAP HYPERSPECTRAL SURVEY

Continuous Surface Mineral Mapping

While drilling and field surveys provide extensive mineralogical data at depth and over very small areas, hyperspectral remote sensing has the capability to provide accurate, continuous mineralogy over very large areas. Hyperspectral imaging or imaging spectroscopy measures the interaction of sunlight with the Earth's surface in order to identify materials such as vegetation and minerals. The many contiguous bands of a hyperspectral imager produce complete spectral signatures that allow for identification of materials rather than simple discrimination afforded by most space-based remote sensing instruments (e.g. Landsat). The high spatial resolution also ensures more accurate surface mapping.

In geothermal exploration, high temperatures, fluid flow and good permeability are the sought after characteristics. The ability to identify and map minerals indicative of high temperature fluid flow is thus coveted as is the ability to map these mineral populations in geographically correct locations. Previous studies have shown that linear distributions of hydrothermal

alteration mineral assemblages are an excellent proxy for faulting, fracturing and/or contact boundary delineation (Martini, 2002; Martini et al., 2003). Particular enlightenment has resulted from comparison of known/previously-mapped faults with those structures mapped via distributions of alteration minerals derived from hyperspectral imaging. In many cases, these two have coincided. Such coincidences target regions experiencing hydrothermal discharge along known faults. As a corollary, portions of faults/fractures not hosting alteration may not currently, or in the near past, be zones of discharge. This information may aid in ruling out certain zones for further exploration. Furthermore, alteration mineralogy's difficult identification in the field means many zones of discharge (either faults, fractures or contacts) can be missed. Hyperspectrally-derived mineral maps can provide a far more complete, unambiguous and efficient mineral mapping service in this regard.

Data Acquisition

Northern Fish Lake Valley was flown on July 4, 2003 with the Australian HyMap sensor (Integrated Spectronics, Ltd.). The hyperspectral survey covered approximately 400 km² between latitude 37°50'49" and 38°2'40" and longitude 118°4'50" and 117°53'59" (see Figure 2A) and took approximately one hour to acquire. It consists of 10 north-south flightlines (1.8 km x 20.5 km) with a nominal spatial resolution of 3 m (which depends on instrument field-of-view and terrain elevation). HyMap samples the electromagnetic spectrum of reflected sunlight from 450-2500 nm wavelength in 126 separate but contiguous wavelength bands from 13 to 17 nm wide. Signal-to-noise ratio (SNR) is well over 1000:1 for most wavelength regions. The instrument was flown aboard a fixed-wing aircraft with complete radiometric and spectral calibration and simultaneous DGPS data acquisition. Data cubes were radiometrically corrected to apparent reflectance using the ATREM algorithm (Gao et al., 1993) and spectrally smoothed using the EFFORT algorithm (Boardman, 1998).

METHODS AND RESULTS

When processing large multi-line datasets such as the Fish Lake Valley survey, it is often advantageous to carry out mineral analysis in two separate tiers. The first tier consists of rapid, robust but simple targeting algorithms that generally rely on non-CPU intensive analysis methods such as band ratio or band indices techniques. These first tier algorithms delineate mineral groups over large areas quickly and serve to target and focus more in-depth mineral mapping efforts and field surveys. The more time and CPU-intensive second tier algorithms are only applied to those regions highlighted in the first mapping algorithm pass as exploration areas of interest. Maps generated from the second-tier algorithms provide detailed, georeferenced, accurate maps of specific minerals in regions of geothermal interest. It is these maps that may delineate primary zones of discharge and reveal hydrothermal geochemistry and general temperatures.

Regional Indices Mapping

The desire to assess larger and larger areas for various resource exploration efforts has driven the size of hyperspectral surveys up to levels that exceed the efficiency of current processing algorithms. In order to address this issue, HyVista Corporation has developed algorithms used to

“spectrally strain” large datasets in order to reduce the data to specific areas of interest in short amounts of time. Though initial field work helps to elucidate hydrothermal flow frameworks, determining places to send geologists and/or determining drilling targets can be challenging over large areas. In the case of Fish Lake Valley, we were able to reduce the data from 400 km² to approximately 25 km² in a little over one hour of processing time.

The cornerstone of the first tier algorithms is band ratios and indices that exploit the unique spectral absorptions of particular earth materials (especially vegetation and minerals). Because the HyMap samples the entire electromagnetic spectrum, we can leverage this by picking out specific bands that bound absorptions of interest and manipulate them mathematically in such a way as to identify and map materials with those particular absorptions over large areas. In order to cut down on computation time and effort, we use band ratios and indices that only rely on two to four bands rather than the more sophisticated algorithms that rely on all the bands and that track the whole spectral signature rather than just locations of principle absorption maxima and minima. This results in maps that highlight regions rich in particular mineral groups but that don’t necessarily absolutely identify specific minerals as the second tier algorithms can do (see Figure 2).

Figure 2A. Georeferenced spatial extent of the 2003 HyMap survey in greyscale. White numbers equal exploration targets of interest as delineated from first-tier indices algorithms. B, C and D are specific mineral group distribution images plotted with local faulting taken from Reheis and Sawyer, 1997. **B.** Kaolinite-rich areas **C.** Mica-rich areas **D.** Carbonate/chlorite-rich areas.

There are more mappable mineral groups, however the three groups shown in Figure 2 have been determined to be some of the most valuable minerals with respect to geothermal exploration. The results of this initial “spectral straining” highlight four areas of potential interest (Figure 2A). They generally fall along the CF, the EPFZ or the intersection between the two, but some isolated populations also occur more centrally in the survey area. All four sites have potential, but site 2 sparked the most interest as it occurs in a structurally interesting position. All four sites will eventually be investigated, but site 2 was processed first and will be discussed in the next section.

Targeted Mineral Mapping

After the Fish Lake Valley survey region was assessed for zones of prospective mineral assemblages, these areas were re-processed using more sophisticated material identification and mapping algorithms that leverage the full spectral capabilities of hyperspectral imaging. As mentioned previously, site 2 appeared to be the most interesting initially. The portion of the survey line containing the majority of the alteration minerals was subset to capture only that area of most interest (Figure 3C shows the extent of the spatial subset in a dashed polygon). This subset was then processed using standard spectral identification and unmixing techniques within the commercially available ENVI software environment. Algorithms that aim to reduce hyperspectral data both spatially and spectrally were applied in order to extract and identify dominant image spectral endmembers. Taken as a whole, these endmembers should explain much of the spectral composition of the original survey line subset.

The dominant spectral signatures extracted from the subset include, but are not limited to, calcite, montmorillinite, kaolinite, dickite, alunite, pyrophyllite, muscovite, illite, jarosite, amorphous silica, epidote and possible diopside. There were also several vegetation signatures that were not included in this analysis and no attempt was made to mask or “zero” any vegetation in this sparse desert environment.

Figure 3A. Local mineral distribution map from the north-eastern portion of the hyperspectral survey. Lines represent faulting from Reheis and Sawyer, 1997. Dashed polygon shows the region highlighted in 3D. **B.** An attempt to clarify and simplify the mineral mapping from 3A. Minerals as defined in legend. **C.** Geology local to the small image subset processed in the second-tier analysis (geology from Reheis and Sawyer, 1997). Thick black lines are faults and finer lines are contact boundaries. The dashed polygon shows the actual boundary of the processed HyMap image. **D.** Close-up of alteration in far northeastern Fish Lake Valley highlighting coincidence of mineral formation along the Os-Tvs contact boundary (dashed line) rather than the main Coaldale Fault (solid line).

Once these signatures were extracted and identified, they were used in sets of mapping algorithms to constrain their spatial distribution within the subset. Due to the difficulty in representing all of the above minerals in a grey-scale environment, only three minerals were chosen for display in Figure 3A, B and D. The advanced-argillic assemblage of montmorillinite, kaolinite and alunite are mapped in Figure 3. The zones populated with alunite also possess small areas of pyrophyllite, however this mineral was not included in this figure for reasons of clarity. Notice that most of the advanced-argillic alteration occurs within the Tertiary volcanic unit (Tvs), though some is also found within the Paleozoic metasediments (Os). Other minerals including muscovite and illite are generally found more in the central and southern part of the image, though some isolated muscovite/illite populations are found along the northern EPFZ. The epidote and calcite are also mostly in the south, but some calcite is found within the Os unit in the north of the image (see Figure 3C for Os location).

DISCUSSION

The results of initial first tier processing were somewhat surprising considering the exploration history of the region. Much of the historical drilling effort and field surveys have been focused on the Tertiary-aged volcanic hills captured in the central and southwestern portion of the hyperspectral survey. The Tvs volcanics in this region were targeted for geothermal drilling in the late 1970's through the 1980's. Steam Reserve Corporation's deep geothermal well drilled in the mid-1980's, found fluids at $> 200^{\circ}\text{C}$ at 2485 m. The company's earlier more shallow well, reached a maximum temperature of 157°C at 600 m (Edmiston and Benoit, 1984). Even earlier, an oil exploration well drilled in 1970 by Nevada Oil and Mining reached a bottom-hole temperature of 159°C at 2775 m. Most of the obvious surface hydrothermal discharge also occurs along the base of the Tvs unit and its intersection with regional Qal deposits in the Fish Lake basin. In addition, hydrothermal discharge seems to have been maintained in this region through at least most of the Pleistocene (Reheis et al., 1993). Couple this with the north to north-northeast trending faults that cut this portion of the Tvs unit, and the area appears to be a prime exploration/exploitation target.

Interestingly, the general mineral assemblage maps shown in Figure 2 target areas other than the previously drilled zones discussed above. There are some weak kaolinite-rich concentrations in

the southern Tvs areas that roughly coincide with faulting, but Figure 2b clearly highlights crust much further to the north along the eastward-trending CF and its intersection with the north-northeast-trending EPFZ (sites 1 and 2).

Second-tier processing in the site 2 area confirms the presence of kaolinite and also reveals a suite of complimentary, advanced argillic minerals that ultimately highlight this region as a primary zone of discharge now or in the past. Mineral mapping in Figure 3 emphasizes classic mineral zonation patterns seen in epithermal mineral deposits and geothermal locales alike. An inner core of high temperature clays and sulfates (alunite) is surrounded by concentrations of slightly lower temperature clays (kaolinite) which are in turn ringed by disseminated low temperature clay (montmorillinite). This pattern is especially obvious in the northern-most section of the data in Figure 3a and b. Though not shown in the mineral maps of Figure 3 (for clarity and presentation reasons), the inner core also possesses pyrophyllite and jarosite. The kaolinite rich areas contain distributions of dickite, muscovite and illite and the montmorillinite zones contain quite a bit of additional amorphous silica.

Spatially, the hydrothermal minerals are mapped within the east-trending CF zone. Extending the tip of the EPFZ northwards towards the CF would place the mineral distributions right in the middle of such an intersection. This possible intersection zone is actually a rather complex structural region. As mentioned earlier, the EPFZ is a right-stepover that transfers strain from the FLVFZ, northeastward into the WLB. Rates of dip-slip on the EPFZ indicate that this set of normal faults is quite active for structures of their kind, experiencing approximately 3 mm/yr of Holocene slip collectively and only 0.2-0.5 mm/yr of right-lateral slip. At northern Fish Lake Valley latitudes, the FLVFZ experiences small amounts of right lateral movement (~2.5 mm/yr) in comparison to average slip along the length of the fault (~5 mm/yr) and accommodates smaller amounts of vertical slip (~0.8 mm/yr). The left-lateral CF also accommodates some of this local extension. The interplay of the above structures produces a significant pull-apart structure in northern Fish Lake Valley. Most of the mapped geothermal alteration lies right at the crux of this transtensional deformation regime. The alteration minerals are likely products of increased hydrothermal fluid flow focused by high rates of extension on normal faults and the intersection of these faults with the east-trending CF. Intersecting faults are known to possess enhanced vertical permeability over non-intersecting solitary structures. Further complexity is revealed in Figure 3c and d where the linear distribution of minerals is revealed to occur not along a portion of the CF, but rather along the Tvs-Os contact. This is not that uncommon in geothermal environments, but it does raise the question as to why fluid flow is preferentially localizing along contacts rather than fault structures. We currently have no explanation for this.

Mica-rich distribution mapped in Figure 2c highlights the same areas as in Figure 2b, but targets even more area along the length of the EPFZ. More specific second-tier mineral mapping reveals extensive distribution of montmorillinite within the EPFZ (Figure 3a and b) as well as isolated occurrences of kaolinite and alunite. Most interesting is that though the distribution of minerals follows the same trend as the EPFZ, it is generally offset approximately 0.5 km to the east of the main EPFZ structure. This probably suggests that the zone between the two main EPFZ structures is actually quite faulted as well. Ultimately, it is important to note that the main discharge structure in this area is not the main strand of the EPFZ, but perhaps secondary structures to the east.

Finally the carbonate/chlorite distribution mapped in Figure 2d mainly highlights those regions where recent hydrothermal spring discharge is occurring or has occurred in the past. This is especially true around site 4 and mid-way in-between sites 1 and 2 (see Figure 2a for site locations). The source of minerals around site 1 is more ambiguous. If it is primarily carbonate, then the source may be primary mineral formation within local Paleozoic sediments. If it is primarily chlorite, then the source may be regional low-temperature hydrothermal alteration or metamorphism. Detailed, second-tier processing will ultimately discriminate the two.

CONCLUSIONS

Airborne hyperspectral data was successfully acquired over northern Fish Lake Valley. The target zones delineated with the quick first-tier algorithms lay mostly in the north along the east-trending CF and its intersection with the north-northeast-trending EPFZ. The intersection of these faults may be the ultimate permeability enhancer. Clearly the transtensional formation of the northern Fish Lake Valley pull-apart basin has also served to focus hydrothermal fluid flow in the region. In such a structural framework, the most intense permeability and flow would be where maximum extension and lateral slip is occurring. This is the Fish Lake Valley pull-apart and specifically the more northerly regions closest to the CF.

The second-tier, in-depth mineral analysis confirmed the presence of high temperature advanced-argillic to argillic alteration minerals. Such mineral suites point to high temperature, acidic source waters at the higher elevations. The second-tier analysis also indicated that fluid flow may be occurring not only within faults but also along contact boundaries and other secondary structures removed from the main faults of the region.

Though field work has yet to be initiated in the Fish Lake Valley region, these first sets of mineral maps provide future exploration efforts with constrained ground targets for in-depth field mapping and/or drilling.

REFERENCES

- Boardman, J., 1998. "ATREM polishing of AVIRIS apparent reflectance data using EFFORT: a lesson in accuracy versus precision." *Summaries of the Seventh Annual JPL Airborne Earth Science Workshop*, 1998.
- Bradley, D.B., D.F. Stockli, J. Lee, N.D. Winters, 2003. "Constraints on the magnitude and rate of Pliocene to recent slip along the left-lateral Coaldale Fault, central Walker Lane Belt, Nevada." *Geological Society of America Abstracts with Programs*, v. 35 (6), September 2003, p. 25.
- Edmiston, R.C. and W.R. Benoit, 1984. "Characteristics of Basin and Range Geothermal Systems with Fluid Temperatures of 150°C to 200°C." *Geothermal Resources Council Transactions*, v.8, p. 417-424.

Gao, B.C., K.B. Heidebrecht, A.F.H. Goetz, 1993. "Derivation of scaled surface reflectances from AVIRIS data." *Remote Sensing of Environment*, v. 44, p. 165-178.

Martini, B.A., 2002. "New insights into the structural, hydrothermal and biological systems of Long Valley Caldera using hyperspectral imaging." PhD thesis, 291 pp., UCSC.

Martini, B.A., E.A. Silver, W.L. Pickles, P.A. Cocks, 2003. "Hyperspectral Mineral Mapping in Support of Geothermal Exploration: Examples from Long Valley Caldera, CA and Dixie Valley, NV, USA." *Geothermal Resources Council Transactions*, v. 27.

Reheis, M.C., J.L. Slate, A. M. Sarna-Wojcicki, C.F. Meyer, 1993. "A late Pliocene to middle Pleistocene pluvial lake in Fish Lake Valley, Nevada and California." *Geological Society of America Bulletin*, v. 105, p. 953-967.

Reheis, M.C. and T.L. Sawyer, 1997. "Late Cenozoic history and slip rates of the Fish Lake Valley, Emigrant Peak, and Deep Springs fault zones, Nevada and California." *Geological Society of America Bulletin*, v. 109 (3), p. 280-299.

Stockli, D.F., T.A. Dumitru, M.O. McWilliams, K.A. Farley, 2003. "Cenozoic tectonic evolution of the White Mountains, California and Nevada." *Geological Society of America Bulletin*, v. 115 (7), p. 788-816.

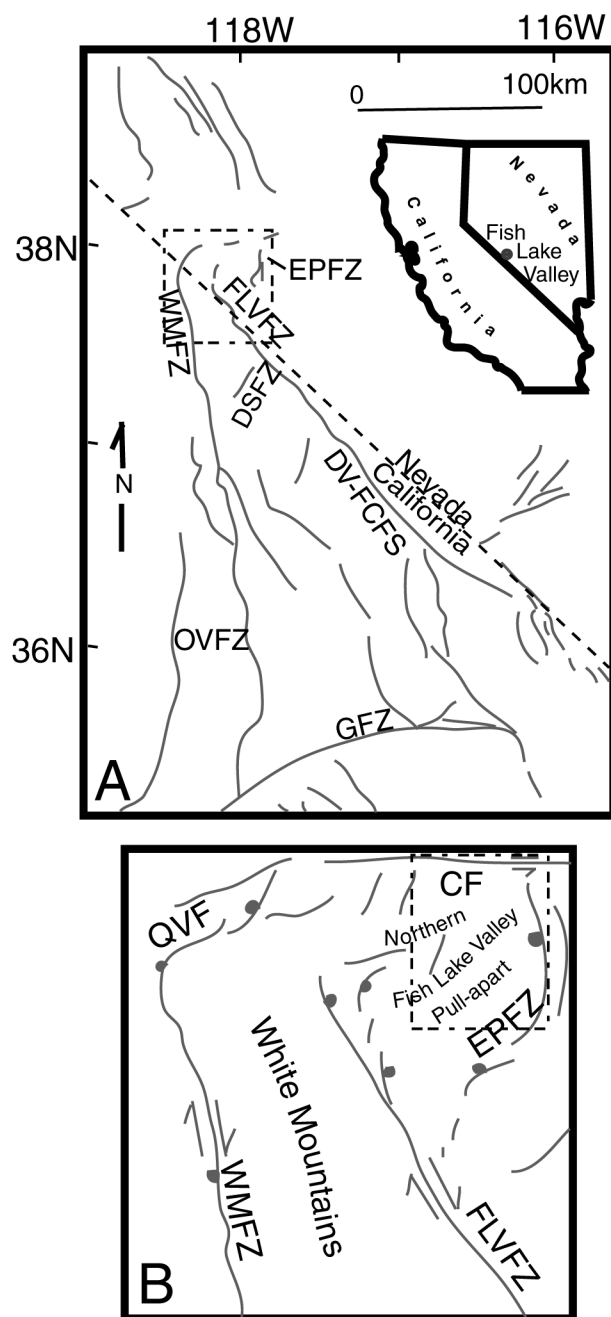


Figure 1.

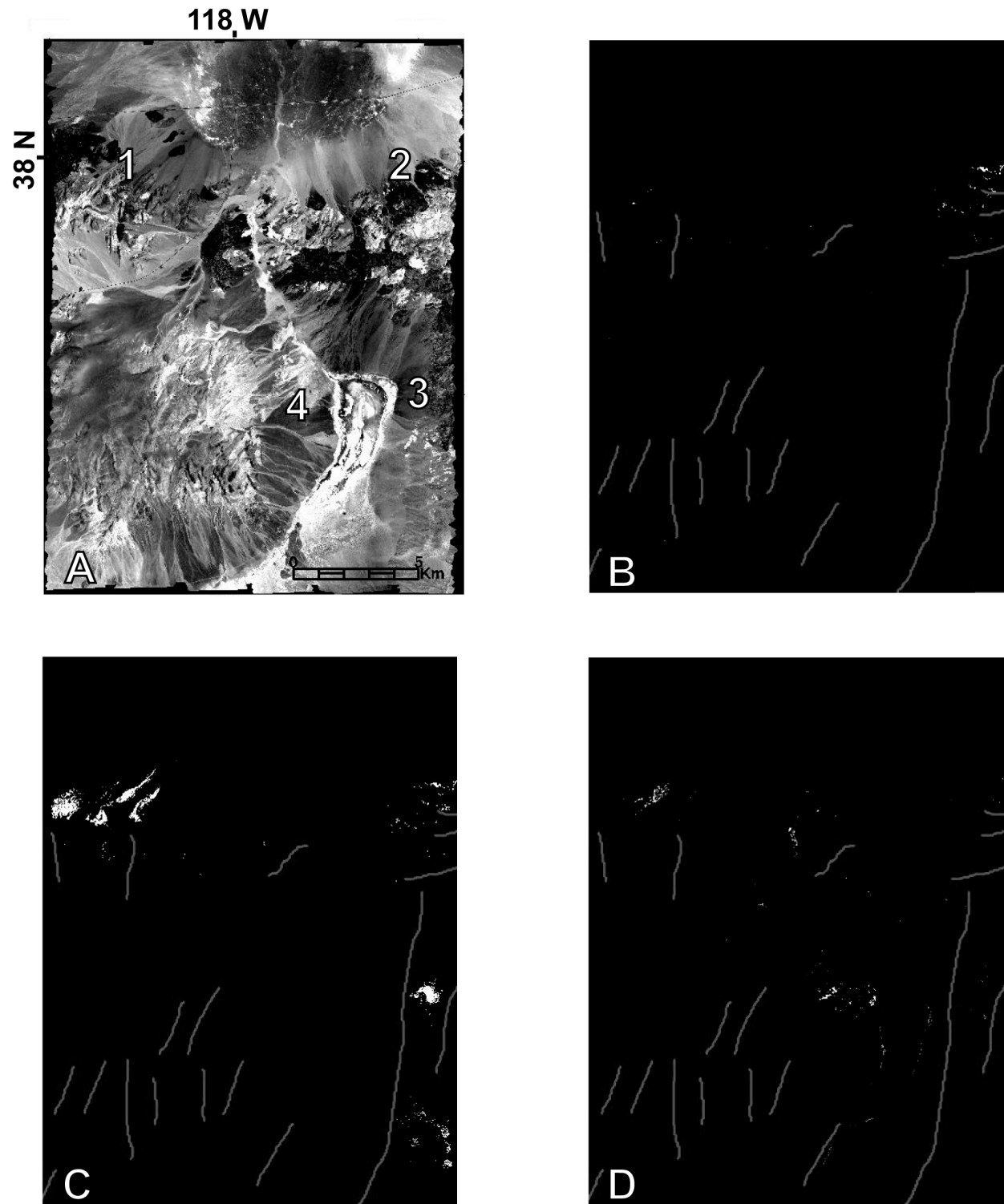


Figure 2.

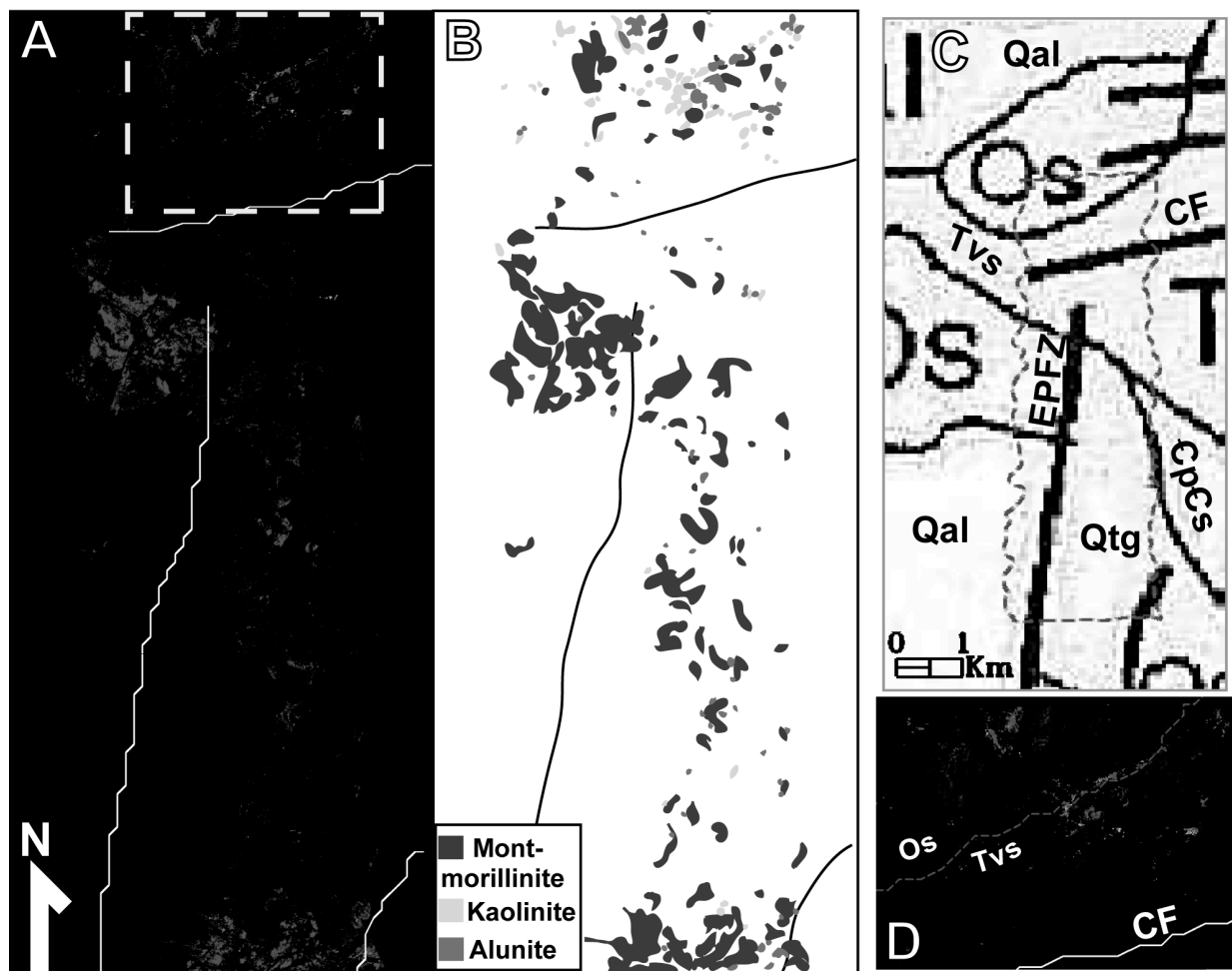


Figure 3.